

Article

Dynamic Mechanical Properties of Ti–Al₃Ti–Al Laminated Composites: Experimental and Numerical Investigation

Jian Ma, Meini Yuan *, Lirong Zheng, Zeyuan Wei and Kai Wang

College of Mechatronic Engineering, North University of China, Taiyuan 030051, China; m821207588@163.com (J.M.); lrzheng1024@163.com (L.Z.); s1901010@st.nuc.edu.cn (Z.W.); s1901008@st.nuc.edu.cn (K.W.)

* Correspondence: mnyuan@nuc.edu.cn; Tel.: +86-035-1392-1795

Abstract: The Ti–Al₃Ti–Al laminated composites with different Al contents were prepared by vacuum hot pressing sintering technology. The effects of Al content on the dynamic mechanical properties of the composites were studied using the combination of Split Hopkinson Pressure Bar experiment and finite element analysis. The results showed that different Al content changes the fracture mode of the composites. The laminated composites without Al have higher brittleness and lower fracture strain. The Ti–Al₃Ti–Al laminated composites containing 10–15%Al have better dynamic mechanical properties than those without Al, but the subsequent increase of Al content is not conducive to the improvement of strength. However, when the Al content in the specimen reaches 30%, the dynamic mechanical properties of the composites decrease, multi-crack phenomenon and relatively large strain occur, and the Al extruded from the layers fills the crack.

Keywords: laminated composites; dynamic compression performance; SHPB; fracture modes



Citation: Ma, J.; Yuan, M.; Zheng, L.; Wei, Z.; Wang, K. Dynamic Mechanical Properties of Ti–Al₃Ti–Al Laminated Composites: Experimental and Numerical Investigation. *Metals* **2021**, *11*, 1489. <https://doi.org/10.3390/met11091489>

Academic Editor: Emin Bayraktar

Received: 28 August 2021

Accepted: 16 September 2021

Published: 19 September 2021

Publisher's Note: MDPI stays neutral with regard to jurisdictional claims in published maps and institutional affiliations.



Copyright: © 2021 by the authors. Licensee MDPI, Basel, Switzerland. This article is an open access article distributed under the terms and conditions of the Creative Commons Attribution (CC BY) license (<https://creativecommons.org/licenses/by/4.0/>).

1. Introduction

Ti–Al₃Ti laminated composites, as a kind of lightweight high performance structure material, are composed of ductile Ti layers and intermetallic compound Al₃Ti layers. Their unique laminated structure and special failure modes make these composites possess excellent dynamic impact resistance. Therefore, the laminated composites are usually used in armor protection, aviation aerospace engineering, and other fields, and have a promising application prospect [1–6].

At present, scholars have researched into the mechanical properties of Ti–Al₃Ti laminated composites, including: three-point bending [7,8], quasi-static compression [9,10], and anti-penetration performance [11–17], etc. Adharapurapu [18] et al., reported that the toughness and fatigue properties of Ti–Al₃Ti laminated composites were improved obviously due to the bridging effect of ductile titanium. Cao [19] et al., through the combination of experiment and simulation, found that the damage modes of Ti–Al₃Ti laminated composites include traverse cracks, crack deflection, and delamination, which enabled the composites to absorb more energy. Zhou [20] et al., found that the fracture modes of the Ti–Al₃Ti interface in the composites varied as a function of strain rate.

It is noted that during the vacuum hot-pressing sintering, different preparation processes would lead to a certain degree of Al still remaining, and form Ti–Al₃Ti–Al laminated composites. Yuan [21] et al., reported that compared to Ti–Al₃Ti laminated composites, Ti–Al₃Ti–Al laminated composites have better static and dynamic compression strength. Price R.D. [22] prepared Ti–Al₃Ti–Al laminated composites by controlling the reactive foils sintering process. The dynamic compression study showed that the composites with 3–15% Al have the best mechanical properties. Du [23] et al., carried out multiple hot rolling of Ti–Al laminated plates at 500 °C and found that the tensile strength of this composite increase with the increasing of the volume fraction of Al. Patselov [24] et al., prepared Ti–Al₃Ti–Al laminated composite with 15% volume fraction Al. Through the three-point

bending experiment, they found that the fatigue signs in the form of grooves were clearly visible in the aluminum layer at the end of the fatigue fracture zone.

The current research mainly focuses on their influence on the overall mechanical properties of laminated composites [25–30], but the systematic studies on the strengthening mechanism of Al are rare. In this study, Ti–Al₃Ti–Al laminated composites were prepared by endothermic semi-solid reaction [31]. The compression behavior and crack propagation of Ti–Al₃Ti–Al laminated composites under high strain rate were studied. The influences of Al layer on the fracture properties were analyzed emphatically. Finally, through finite element simulation, the influences of different Al contents on the dynamic mechanical properties of Ti–Al₃Ti–Al laminated composites were analyzed.

2. Experimental Method

2.1. Materials Preparation

Ti–Al₃Ti–Al laminated composites were prepared by the hot-pressing sintering method. Al alloy foils and TC4 alloy foils of different thickness were used as the initial components of the Ti–Al₃Ti–Al laminated composites. The compositions of TC4 alloy foils and Al alloy foils are shown in Table 1. The processed and cleaned TC4 foils and Al foils were stacked alternately, then placed in the hot-pressing sintering furnace (ZT-40-21Y, Shanghai Chenhua Science Technology CO. Ltd, Shanghai, China). The temperature was then raised to 600–710 °C. The Ti–Al₃Ti–Al laminated composites with residual Al were obtained by adjusting the thickness ratio of the laminates and controlling the heat preservation time. The prepared materials were cut into $\varnothing 8$ mm cylindrical specimens through the line cutting process.

Table 1. TC4 and Al alloy composition (mass fraction) %.

Alloy	TC4	Alloy	Al
Al	5.50–6.75	Si	≤0.5
V	3.5–4.5	Fe	≤0.5
Fe	≤0.5	Cu	3.8–4.9
C	≤0.1	Mn	0.30–0.9
O	≤0.2	Mg	1.2–1.8
N	≤0.05	Ni	≤0.1

2.2. Mechanical Experiment

The Split Hopkinson Pressure Bar (SHPB) (Harbin Institute of Technology, Harbin, China) experiment is one of the most important research methods to investigate the dynamic mechanical properties of the material at strain rates of 10^2 – 10^4 S^{−1}. The diameter and the length of the bar were 12 mm and 1200 mm, respectively. The specimen was 8 mm in diameter and 6 mm in thickness. The SHPB apparatus consists of a high pressure air gun, a striker bar, an incident bar, and a transmitter bar as shown in Figure 1.

The impact bar launched by the high-pressure air gun impacted the input bar axially and resulted in the formation of loading pulse, which propagated along the bar to the specimen. The specimen then deformed under the action of the pulse. Meanwhile, the reflection pulse was transmitted back to the incident bar, and the transmission pulse was transmitted to the transmission bar. The gauge at the center of the bar was used to record the strain. The incident, reflected, and transmitted signals were recorded on the oscilloscope in the form of voltage, and the voltage was converted to the actual incident ε_i , reflected ε_r and transmitted ε_t .

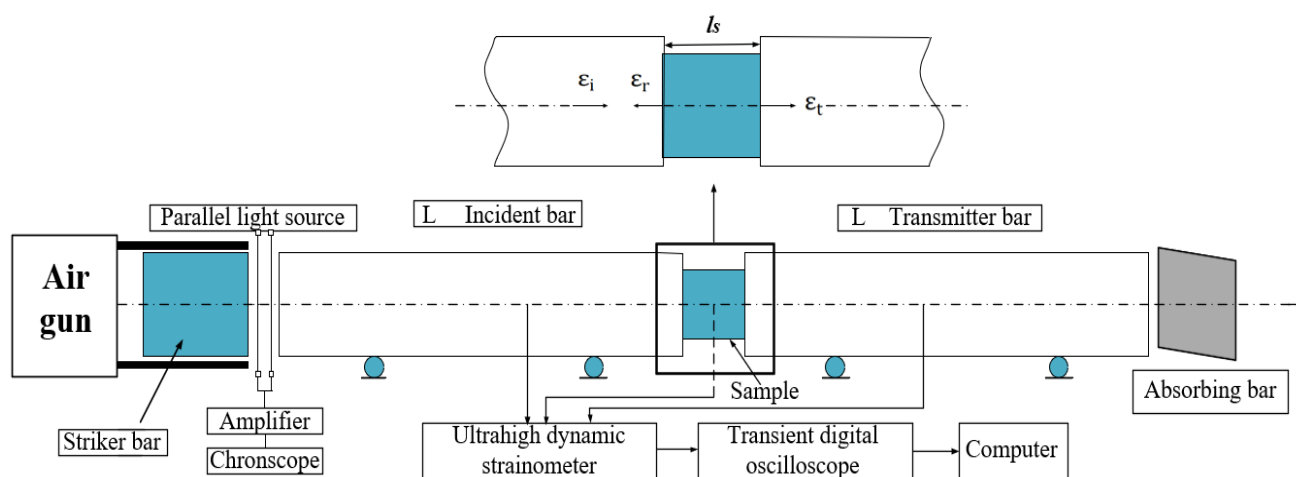


Figure 1. Schematic of a Split Hopkinson pressure bar apparatus.

Then the pattern strain rate $\dot{\varepsilon}_s$, strain σ_s , and stress ε_s were:

$$\dot{\varepsilon}_s = \frac{d\varepsilon_s}{dt} = \frac{C_0}{l_0} (\varepsilon_i - \varepsilon_r - \varepsilon_t) \quad (1)$$

$$\sigma_s = \frac{EA}{2A_s} (\varepsilon_i + \varepsilon_r + \varepsilon_t) \quad (2)$$

$$\varepsilon_s = \frac{C_0}{l_s} \int_0^{t_0} (\varepsilon_i - \varepsilon_r - \varepsilon_t) dt \quad (3)$$

where: A_s is the cross-sectional area of the test piece, and l_s is the thickness of the test piece. C_0 is the elastic longitudinal wave velocity of the waveguide rod.

The main equipment parameters are: high-strength steel was selected for all the bars, the elastic modulus is 200 GPa, the density is 7800 cm/m³, and Poisson's ratio is 0.29. The length of the impact bar is 200 mm, and the length of the incident bar and transmission bar is 1200 mm. The impact rate is 35 m/s.

2.3. Numerical Simulation Method

Ansys LS-DYNA (Ansys 17.0 LS-DYNA, Ansys Inc., Pittsburgh, PA, USA) was used to simulate the Split Hopkinson Pressure Bar experiment and study the dynamic mechanical properties of Ti–Al₃Ti–Al laminated composites. Both the Split Hopkinson Pressure Bar and the impacted specimen are cylindrical, so the three-dimensional axisymmetric finite element model was established (Figure 2) using the APDL command stream. As shown in Figure 2b, the laminated composite model consists of Al layers, Ti layers, and Al₃Ti layers. To make the calculation process smoother and the calculation results more accurate, SOLID 185 elements were selected to represent Al layers, Ti layers, and Al₃Ti layers. A common node setting was adopted to simulate the interface combination. Ti layers, Al₃Ti layers, and Al layers in laminated composites were meshed with different amounts of quadrilateral elements in terms of their thickness. The total number of elements was around 43,200, the time per step is 1 μs.

The bar and specimen were simplified into coaxial cylinders. To reduce errors, mesh encrypted treatment was carried out on the bar near the specimen. The diameter of the bullet was 12 mm and its length was 20 mm, and the speed was set to 30 m/s. The diameter and the length of the bar were 12 mm and 1200 mm, respectively. The specimen was 8 mm in diameter and 6 mm in thickness. The dimensions of each layer of the model are shown in Table 2. The model without Al contains 25 TC4 layers and 24 Al₃Ti layers (Model 1), the other models contain 24 layers of Al, 25 layers of TC4, and 48 layers of Al₃Ti.

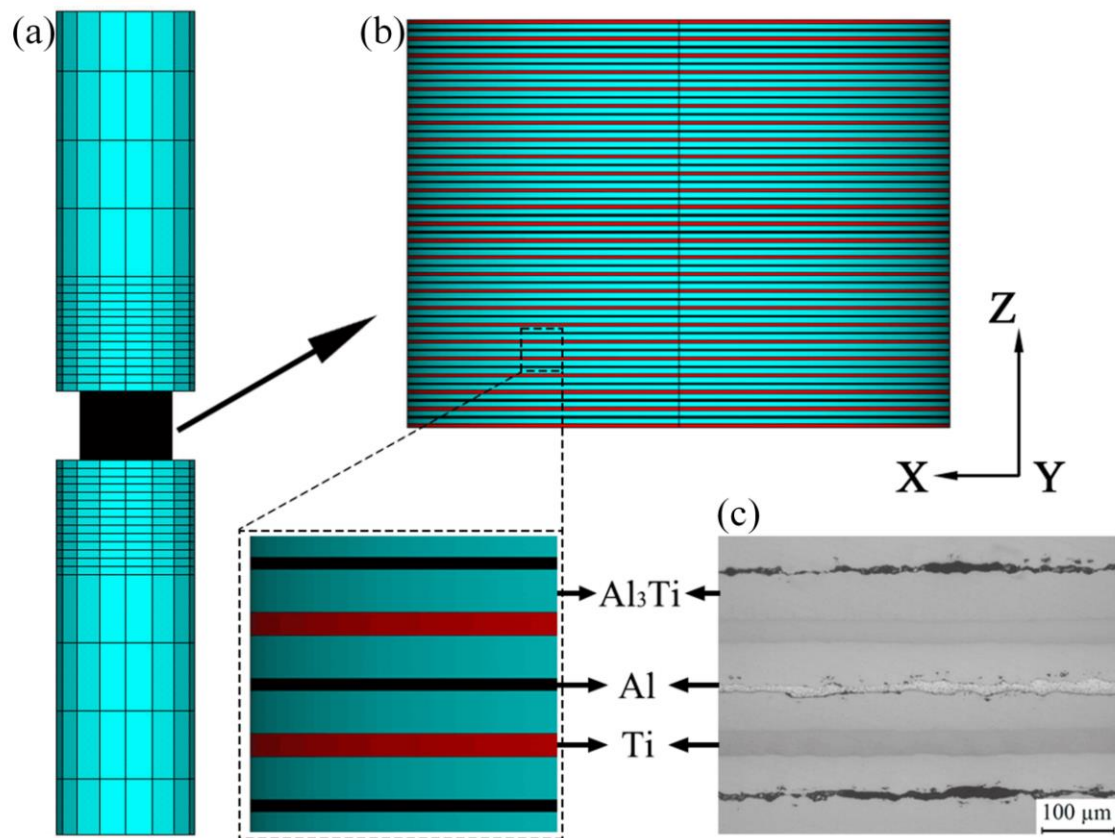


Figure 2. (a) The finite element mesh SHPB experiment system (local), (b) Finite element model of Ti–Al₃Ti–Al specimen, (c) Metallographic diagram of Ti–Al₃Ti–Al specimen.

Table 2. Size parameters of the target model containing different percentages of Al.

-	Thickness and Number of Al Alloy Layers (μm/n)	Thickness and Number of TC4 Alloy Layers (μm/n)	Thickness and Number of Al ₃ Ti Alloy Layers (μm/n)	Proportion of Al Content (%)
Model 1	0/0	48/25	200/24	0
Model 2	25/24	48/25	87.5/48	10
Model 3	50/24	48/25	75/48	20
Model 4	75/24	48/25	62.5/48	30

The JOHNSON–COOK constitutive model and Mie–Gruneisen state equation were used to model TC4 and Al plates. Detailed parameters are shown in Table 3 [32,33].

Table 3. Material parameters of TC4 and Al layers [32,33].

-	P (g/cm ³)	E (GPa)	ν	A (GPa)	B (GPa)	C	m	n	T melt (K)
Al	2.71	71	0.34	265	426	0.015	1.1	0.93	-
TC4	4.428	113.8	0.342	1098	1092	0.014	1.1	0.93	1878

The Johnson–Holmquist–Ceramics (JH-II) [34] constitutive model was used to describe the brittle Al₃Ti material; the specific parameters are shown in Table 4 [32].

Table 4. Material parameters of Al₃Ti layers [32].

P (g/cm ³)	E (GPa)	ν	A	B	C	M	N	T	PHEL (GPa)
3.35	216	0.17	0.85	0.31	0.013	0.21	0.29	0.2	1.842
D1	D2	K1 (GPa)	K2 (GPa)	K3 (GPa)	-	-	-	-	-
0.02	1.85	2.01	2.6	0	-	-	-	-	-

3. Results and Discussion

3.1. Dynamic Mechanical Properties

Figure 3 shows the dynamic compressive stress–strain curves of Ti–Al₃Ti–Al laminated composites with different Al contents. The maximum peak stresses of 0%, 15%, and 30%Al content are 1156 MPa, 1175 MPa, and 927 MPa, respectively, and the fracture strain is 0.094, 0.103, and 0.122 respectively. It can be seen that Ti–Al₃Ti–Al laminated composite with 15% Al content shows a higher compressive strength. When Al contents increase from 0% to 15%, the fracture strain increases by 9.6%. While when Al contents increase from 15% to 30%, the fracture strain increases by 18.4%.

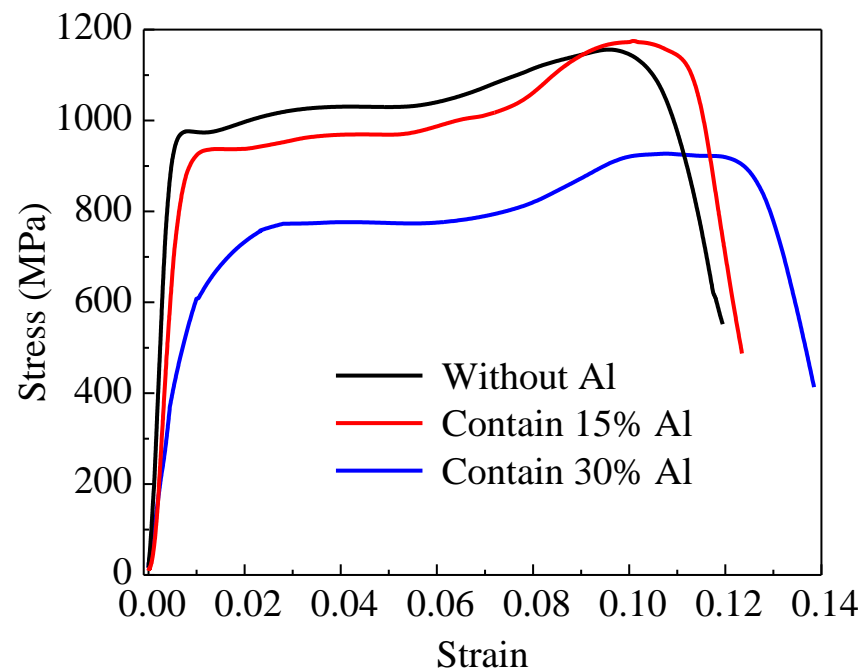


Figure 3. Dynamic compressive stress–strain curves of Ti–Al₃Ti–Al laminated composites with different Al contents.

In the strain range of 0–0.01, the stress growth rate gradually decreases with the increase of Al contents, indicating that the presence of Al makes the specimen need more strain to achieve compactness. In the strain range of 0.02–0.08, the stress–strain curves of the specimens are relatively flat due to the significant thermal softening effect of Al that counteracted the effect of strain hardening [35,36]. Some studies [37] have shown that the plastic deformation of aluminum alloys at high strain rates is mainly characterized by adiabatic heating and shear strain localization.

The fracture characteristics of the specimens with different Al contents impacted by SHPB are shown in Figure 4. For the specimen without Al (Figure 4a), the obvious brittleness fracture is occurred, and three cracks appear on the surface.

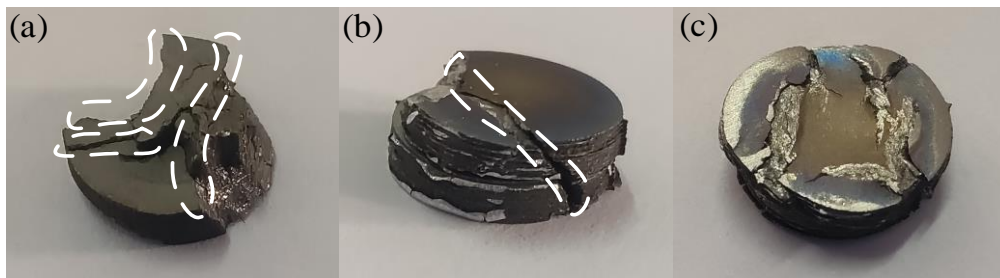


Figure 4. The specimen after fracture and the fracture morphology observed under electron microscope: (a) Without Al, (b) containing about 15% Al, (c) containing about 30% Al.

For the specimen containing about 15% Al (Figure 4b), it can be seen that there is only one main crack on the surface, about 45° to the axis, which means the shear fracture occurred in the specimen. A small amount of Al extrudes from the layer.

For the specimen containing about 30% Al (Figure 4c), the multi-cracks phenomenon appeared in the specimen and caused the whole specimen to fracture. Large amounts of Al are squeezed out of the cracks. The deformation degree of the specimen is large.

By contrast, the brittleness of the specimen without Al is relatively large. The specimen with 15% Al has the best impact resistance. Huang's research [30] found that local plastic deformation of the Al layer slows down excessive interlayer residual stress. Price's research [22] also showed that residual Al can slow down Al₃Ti damage and prevent separation.

3.2. Simulation Calculation

3.2.1. The Simulated Dynamic Stress-Strain Curves

Figure 5 shows the simulated dynamic stress–strain curves of Ti–Al₃Ti–Al laminated composites with different Al contents. The compressive strength of the material with 0%, 10%, 20%, and 30% Al content is 1166.0 MPa, 1181.4 MPa, 1025.2 MPa, and 913.3 MPa respectively, and the fracture strain is 0.090, 0.095, 0.113, and 0.145 respectively. For the Ti–Al₃Ti–Al laminated composites with 10% Al content (Ti:Al₃Ti:Al = 2:7:1), its fracture strain is greater than that of the materials without Al, and its compressive strength is the highest. It has a good balance between brittleness and toughness. When the Al content is 20%, the compressive strength of the material decreases by 13.2% compared with that of 10% Al, but the fracture strain increases by 18.9%. When the Al content increases to 30%, the compressive strength continues to decrease and the fracture strain continues to increase. Konieczny [38] also pointed out that the amount of residual aluminum on the intermetallic compound centerline increased the ductility of the composites.

3.2.2. Energy Analysis

Figure 6a shows the energy variation curves of the specimens with different Al contents during the SHPB experiment. The time of 0 μs is the time when the incident wave just contacts the specimen. The total energy absorbed by the specimens with 0%, 10%, 20%, and 30% Al content is 29.03 J, 30.29 J, 35.49 J, and 39.88 J, respectively. It can be seen that with the increase of Al content, the energy absorbed by the specimen increases gradually. This indicates that the higher the Al content, the stronger the energy absorption capacity of the laminated composites. After the energy absorption reaches the peak, there is a small decline. This is due to the recovery of elastic deformation and energy release of the specimen.

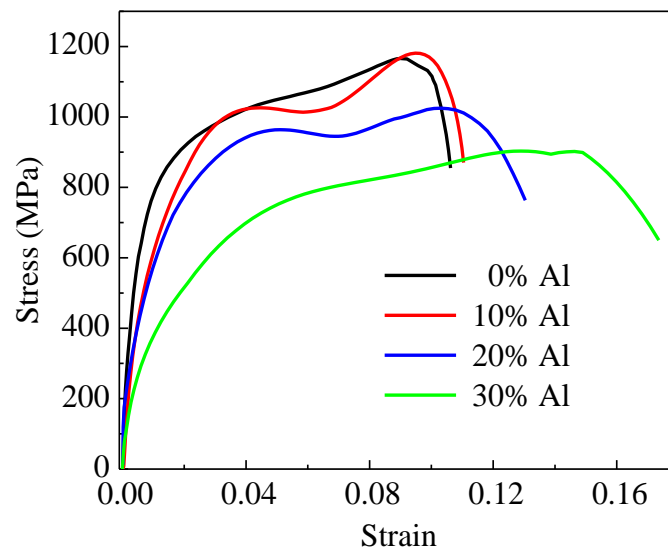


Figure 5. The simulated dynamic stress-strain curves of Ti–Al₃Ti–Al laminated composites with different Al contents.

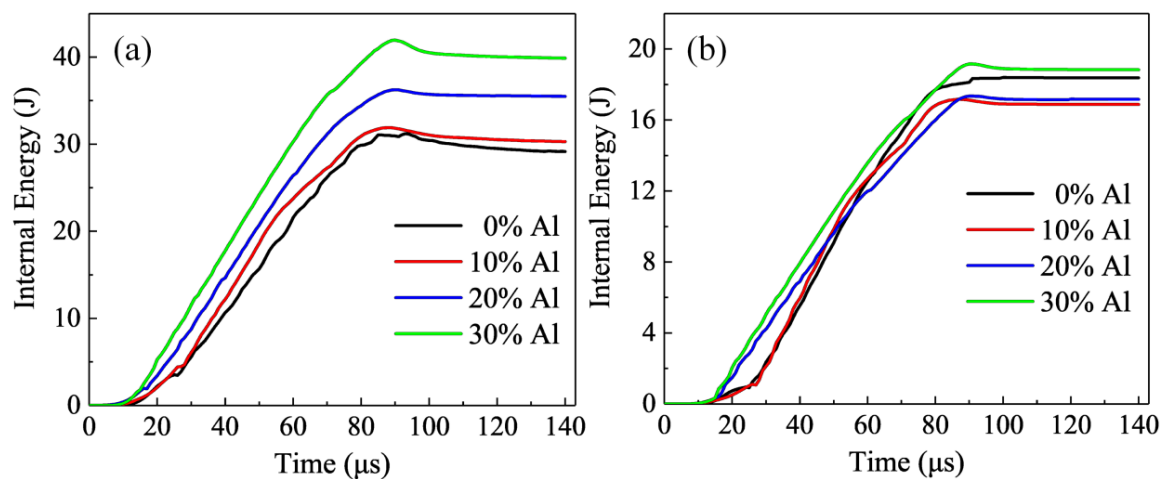


Figure 6. Energy absorption–time curves of Ti–Al₃Ti–Al laminated composites with different Al contents: (a) the whole; (b) Ti layers.

For the Ti layers of the composites (Figure 6b), with the increase of Al content, the energy absorption of the Ti layer is 18.38 J, 16.88 J, 17.02 J, and 19.30 J, respectively. It can be seen that the energy absorbed by the Ti layers in the Ti–Al₃Ti–Al laminated material containing 10% Al is the lowest. However, the energy absorption of Ti layers in the laminated composites without Al is higher than that of 10% Al and 20% Al. In addition, although the volume fraction of the Ti layer only accounts for 20%, its energy absorption is about half of the total energy absorption, which indicates that the ductile layer Ti is the main energy absorption layer, increasing the toughness of laminated composites.

Figure 7 shows the deformation degree of the Ti layer of Ti–Al₃Ti–Al laminated composites with different Al contents. It can be seen that with the increase of Al content, the maximum strain of the Ti layer in each sample is 0.498, 0.434, 0.445, and 0.537, respectively. The strain of Ti is the lowest at 10% Al content, indicating that the risk of fracture of the composites is low. This corresponds to the result of Figure 7b above.

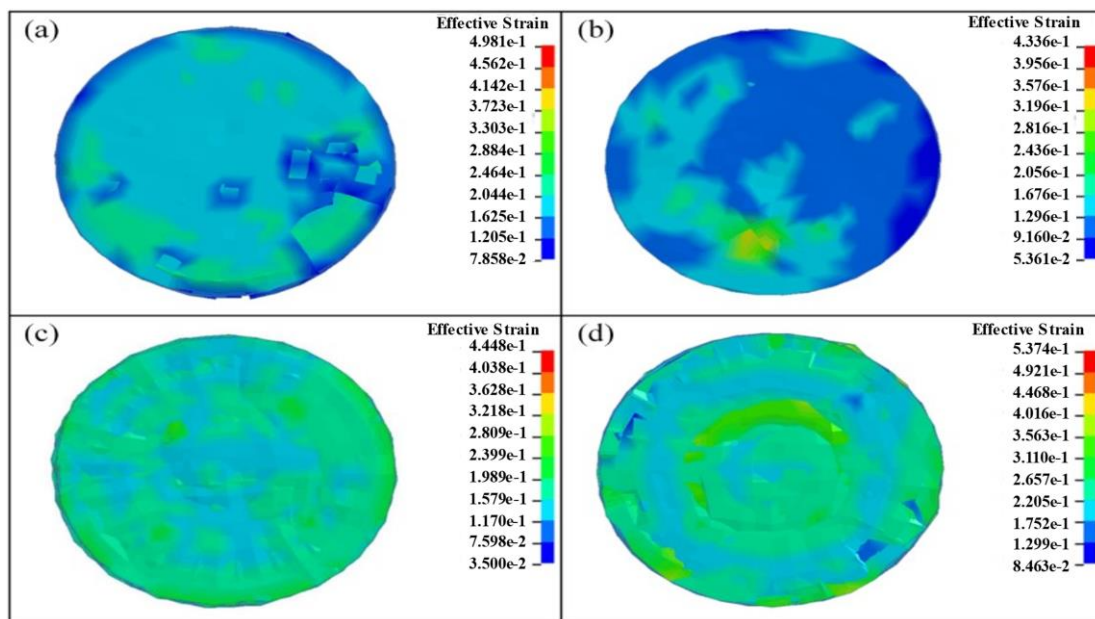


Figure 7. The deformation degree of Ti layer in Ti–Al₃Ti–Al laminated composites with different Al contents: (a) 0% Al, (b) 10% Al, (c) 20% Al, (d) 30%.

3.2.3. Comparison of Failure Morphology

Figure 8 shows the stress nephogram of the longitudinal section of the specimen after impact. Different Al contents lead to different deformation degrees and failure mode of the specimen. It can be seen that Ti–Al₃Ti–Al laminated composites containing 10% Al have the best protective performance under dynamic impact.

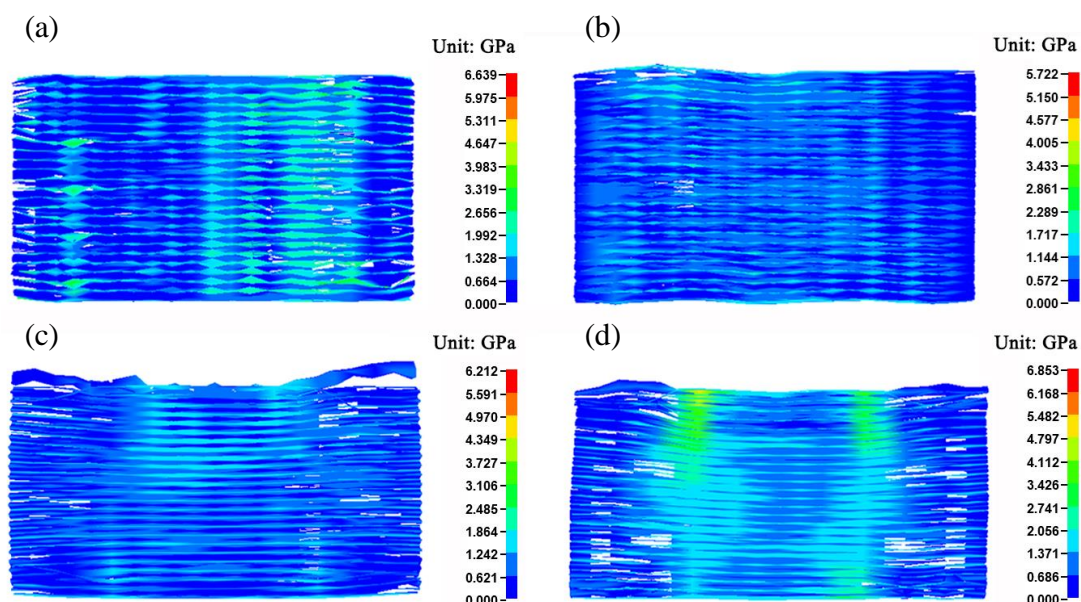


Figure 8. Stress nephogram of longitudinal section of Ti–Al₃Ti–Al laminated composites with different Al contents: (a) 0% Al, (b) 10% Al, (c) 20% Al, (d) 30%.

For the specimen without Al (Figure 8a), the stress distribution is not uniform and a large number of microcracks are generated. However, the Ti layer can effectively prevent the propagation of microcracks, thus the specimen has no overall failure.

For the specimen containing 10% Al (Figure 8b), the whole specimen is relatively intact with few failure units, indicating that Al plays a positive role in it. The overall

stress distribution of the specimen is uniform, and there is no high-stress concentration phenomenon.

When the Al content reaches 20% (Figure 8c), the interlayer stress increases, and the phenomenon of stratification occurs.

When the Al content reaches 30% (Figure 8d), more failure elements appear in the specimen, indicating that large cracks have formed, because with the increase of Al content, the strength and stiffness of the material decrease, and the ability of resisting impact load weakens.

4. Conclusions

The dynamic mechanical properties of Ti–Al₃Ti–Al laminated composites were studied by SHPB experiment and numerical simulation. The conclusions can be summarized as follows:

- (1) The Ti–Al₃Ti–Al laminated composites with Al content of 10–15% had excellent compressive strength and failure strain.
- (2) The laminated composites without Al showed brittle fracture; there were three main cracks on the surface of the specimen. The laminated composites containing 15% Al had only one main crack, and ruptured in a direction approximately 45° from the vertical axis. When the Al content reached 30%, the specimen revealed multiple cracking properties, and the deformation was large.
- (2) When the Al content was 10%, the overall stress distribution of the specimen was uniform and had the best impact resistance.

Author Contributions: Conceptualization, Methodology, J.M.; Project administration, Writing—review & editing, M.Y.; Investigation, L.Z.; Visualization, Z.W.; Supervision, Validation, Funding acquisition, K.W. All authors have read and agreed to the published version of the manuscript.

Funding: The authors acknowledge the financial supports provided by the National Natural Science Foundation of China (51201155), the Natural Science of Shanxi Province (2012011019-1, 2012011007-1), the Chinese Education Ministry Foundation for Doctors (20101420120006), and the National Key Research and Development Program of China (2018YFC1901704).

Institutional Review Board Statement: Not applicable.

Informed Consent Statement: Not applicable.

Data Availability Statement: The raw/processed data required to reproduce these findings cannot be shared at this time due to technical or time limitations.

Conflicts of Interest: The authors declare no conflict of interest.

References

1. Yang, D.K.; Cizek, P.; Hodgson, P.; Wen, C.E. Ultrafine equiaxed-grain Ti/Al composite produced by accumulative roll bonding. *Scr. Mater.* **2010**, *62*, 321–324. [[CrossRef](#)]
2. Milman, Y.V.; Miracle, D.B.; Chugunova, S.I.; Voskoboinik, I.V.; Podrezov, Y.N. Mechanical behaviour of Al₃Ti intermetallic and 112 phases on its basis. *Intermetallics* **2001**, *9*, 839–845. [[CrossRef](#)]
3. Foadian, F.; Soltanieh, M.; Adeli, M.; Etmianbakhsh, M.A. Study on the Formation of Intermetallics During the Heat Treatment of Explosively Welded Al-Ti Multilayers. *Metall. Mater. Trans. A* **2014**, *45*, 1823–1832. [[CrossRef](#)]
4. Rohatgi, A.; Harach, D.J.; Vecchio, K.S.; Harvey, K.P. Resistance-curve and fracture behavior of Ti–Al₃Ti metallic–intermetallic laminate (MIL) composites. *Acta Mater.* **2003**, *51*, 2933–2957. [[CrossRef](#)]
5. Suzuki, A.; Kosugi, N.; Takata, N.; Kobashi, M. Microstructure and compressive properties of porous hybrid materials consisting of ductile Al/Ti and brittle Al₃Ti phases fabricated by reaction sintering with space holder. *Mater. Sci. Eng.* **2020**, *776*, 139000. [[CrossRef](#)]
6. Yang, R.; Zhao, F.; Wang, L.Z.; Zhang, Z.Y.; Zhang, B.B. Fast fabrication of Al₃Ti/Al composites using combustion synthesis and melt dilution. *Mater. Lett.* **2021**, *298*, 130036. [[CrossRef](#)]
7. Peng, L.; Li, H.; Wang, J. Processing and mechanical behavior of laminated titanium–titanium tri-aluminide (Ti–Al₃Ti) composites. *Mat. Sci. Eng. A* **2005**, *406*, 309–318. [[CrossRef](#)]
8. Adharapurapu, R.R.; Vecchio, K.S.; Jiang, F.C.; Rohatgi, A. Fracture of Ti–Al₃Ti metal–intermetallic laminate composites: Effects of lamination on resistance-curve behavior. *Metall. Mater. Trans. A* **2005**, *36*, 3217–3236. [[CrossRef](#)]

9. Li, T.Z.; Grignon, F.; Benson, D.J.; Vecchio, K.S.; Olevsky, E.A.; Jiang, F.C.; Rohatgi, A.; Schwarz, R.B.; Meyers, M.A. Modeling the elastic properties and damage evolution in Ti–Al₃Ti metal–intermetallic laminate (MIL) composites. *Mat. Sci. Eng. A* **2004**, *374*, 10–26. [[CrossRef](#)]
10. Li, T.Z.; Jiang, F.C.; Olevsky, E.A.; Vecchio, K.S.; Meyers, M.A. Damage evolution in Ti₆Al₄V–Al₃Ti metal–intermetallic laminate composites. *Mat. Sci. Eng. A* **2007**, *443*, 1–15. [[CrossRef](#)]
11. Fan, X.L.; Yuan, M.N.; Qin, Q. Failure mechanisms of Ti–Al₃Ti metal–intermetallic laminate composites under high-speed impact. *Rare. Metal. Mat. Eng. A* **2018**, *47*, 2615–2620.
12. Pereira, J.M.; Revilock, D.M.; Ruggeri, C.R.; Emmerling, W.C.; Altobelli, D.J. Ballistic Impact Testing of Aluminum 2024 and Titanium 6Al–4V for Material Model Development. *J. Aerospace Eng.* **2014**, *27*, 56–465. [[CrossRef](#)]
13. Vecchio, K.S. Synthetic multifunctional metallic–intermetallic laminate composites. *JOM* **2005**, *57*, 25–31. [[CrossRef](#)]
14. Snipes, J.S.; Ramaswami, S.; Grujicic, M. Penetration resistance and ballistic–impact behavior of Ti/TiAl₃ metal/intermetallic laminated composites (MILCs): A computational investigation. *Aims. Mater. Sci.* **2016**, *3*, 686–721.
15. Zelepugin, S.A.; Zelepugin, A.S.; Tolkachev, V.F. Numerical Simulation of Multilayer Composites Failure under Dynamic Loading. *Appl. Mech. Mater.* **2015**, *756*, 408–413. [[CrossRef](#)]
16. Zelepugin, S.A.; Mali, V.I.; Zelepugin, A.S.; Ilina, E. Failure of Metallic–Intermetallic Laminate Composites under Dynamic Loading. *AIP Conf. Proc.* **2012**, *1426*, 1101–1104.
17. Harach, D.J. Processing, properties, and ballistic performance of titanium–aluminum titanium metal–intermetallic laminate (MIL) composites. *Diss. Abstr. Int.* **2000**, *61*, 4922.
18. Adharapurapu, R.R.; Vecchio, K.S.; Jiang, F.C.; Rohatgi, A. Effects of ductile laminate thickness, volume fraction, and orientation on fatigue–crack propagation in Ti–Al₃Ti metal–intermetallic laminate composites. *Metall. Mater. Trans. A* **2005**, *36*, 95–1608. [[CrossRef](#)]
19. Cao, Y.; Guo, C.H.; Zhu, S.F.; Wei, N.X.; Javed, R.A.; Jiang, F.C. Fracture behavior of Ti/Al₃Ti metal–intermetallic laminate (MIL) composite under dynamic loading. *Mat. Sci. Eng. A* **2015**, *637*, 235–242. [[CrossRef](#)]
20. Zhou, P.J.; Guo, C.H.; Wang, E.H.; Wang, Z.M.; Chen, Y.; Jiang, F.C. Interface tensile and fracture behavior of the Ti/Al₃Ti Metal–Intermetallic Laminate (MIL) composite under quasi–static and high strain rates. *Mat. Sci. Eng. A* **2016**, *665*, 66–75. [[CrossRef](#)]
21. Yuan, M.N.; Yao, Y.H.; Han, F.Z.; Wang, Z.J. Evaluation of the compressive and anti–penetration properties of Ti–Al₃Ti–Al laminated composites. *Adv. Compos. Lett.* **2020**, *29*, 1–5. [[CrossRef](#)]
22. Price, R.D.; Jiang, F.C.; Kulin, R.M.; Vecchio, K.S. Effects of ductile phase volume fraction on the mechanical properties of Ti–Al₃Ti metal–intermetallic laminate (MIL) composites. *Mater. Sci. Eng. A* **2011**, *528*, 3134–3146. [[CrossRef](#)]
23. Du, Y.; Fan, G.H.; Yu, T.B.; Hansen, N.; Geng, L.; Huang, X.X. Laminated Ti–Al composites: Processing, structure and strength. *Mater. Sci. Eng. A* **2016**, *673*, 572–580. [[CrossRef](#)]
24. Patselov, A.M.; Gladkovskii, S.V.; Lavrikov, R.D.; Kamantsev, I.S. Fracture toughness of Ti–Al₃Ti–Al–Al₃Ti laminate composites under static and cyclic loading conditions. *Russ. Metall.* **2015**, *2015*, 811–815. [[CrossRef](#)]
25. Chen, W.H.; He, W.J.; Chen, Z.J.; Jiang, B.; Liu, Q. Extraordinary room temperature tensile ductility of laminated Ti/Al composite: Roles of anisotropy and strain rate sensitivity. *Int. J. Plast.* **2020**, *133*, 102806. [[CrossRef](#)]
26. Harach, D.J.; Vecchio, K.S. Microstructure evolution in metal–intermetallic laminate (MIL) composites synthesized by reactive foil sintering in air. *Metall. Mater. Trans. A* **2001**, *32*, 1493–1505. [[CrossRef](#)]
27. Wu, H.; Cui, X.P.; Geng, L.; Fan, G.H.; Pang, J.C.; Wei, L.S. Fabrication and characterization of in–situ TiAl matrix composite with controlled microlaminated architecture based on SiC/Al and Ti system. *Intermetallics* **2013**, *43*, 8–15. [[CrossRef](#)]
28. Peng, L.M.; Wang, J.H.; Li, H.; Zhao, J.H.; He, L.H. Synthesis and microstructural characterization of Ti–Al₃Ti metal–intermetallic laminate (MIL) composites. *Scripta. Mater.* **2005**, *52*, 243–248. [[CrossRef](#)]
29. Fan, M.Y.; Domblesky, J.; Jin, K.; Qin, L.; Cui, S.Q.; Guo, X.Z.; Kim, N.; Tao, J. Effect of original layer thicknesses on the interface bonding and mechanical properties of TiAl laminate composites. *Mater. Des.* **2016**, *99*, 535–542. [[CrossRef](#)]
30. Huang, M.; Xu, C.; Fan, G.H.; Maawad, E.; Gan, W.M.; Geng, L.; Lin, F.X.; Tang, G.Z.; Wu, H.; Du, Y.; et al. Role of layered structure in ductility improvement of layered Ti–Al metal composite. *Acta Mater.* **2018**, *153*, 235–249. [[CrossRef](#)]
31. Yuan, M.N.; Li, L.L.; Wang, Z.J. Study of the microstructure modulation and phase formation of Ti–Al₃Ti laminated composites. *Vacuum.* **2018**, *157*, 481–486. [[CrossRef](#)]
32. Cao, Y.; Zhu, S.F.; Guo, C.H.; Vecchio, K.S.; Jiang, F.C. Numerical Investigation of the Ballistic Performance of Metal–Intermetallic Laminate Composites. *Appl. Compos. Mater.* **2015**, *22*, 437–456. [[CrossRef](#)]
33. Senthil, K.; Arindam, B.; Iqbal, M.A.; Gupta, N.K. Ballistic Response of 2024 Aluminium Plates Against Blunt Nose Projectiles. *Procedia Eng.* **2017**, *173*, 363–368. [[CrossRef](#)]
34. Holmquist, T.J.; Johnson, G.R. Modeling prestressed ceramic and its effect on ballistic performance. *Int. J. Impact. Eng.* **2005**, *31*, 113–127. [[CrossRef](#)]
35. Tiamiyu, A.A.; Basu, R.; Odeshi, A.G.; Szpunar, J.A. Plastic deformation in relation to microstructure and texture evolution in AA 2017–T451 and AA 2624–T351 aluminum alloys under dynamic impact loadings. *Mater. Sci. Eng. A* **2015**, *636*, 379–388. [[CrossRef](#)]
36. Xiong, Y.Y.; Li, N.; Jiang, H.W.; Li, Z.G.; Xu, Z.; Liu, L. Microstructural Evolutions of AA7055 Aluminum Alloy Under Dynamic and Quasi–static Compressions. *Acta Metall. Sin. Engl.* **2014**, *27*, 272–278. [[CrossRef](#)]

-
37. Odeshi, A.G.; Adesola, A.O.; Badmos, A.Y. Failure of AA 6061 and 2099 aluminum alloys under dynamic shock loading. *Eng. Fail. Anal.* **2013**, *35*, 302–314. [[CrossRef](#)]
 38. Konieczny, M. Relations between Microstructure and Mechanical Properties in Laminated Ti-Intermetallic Composites Synthesized Using Ti and Al Foils. *Key. Eng. Mater.* **2013**, *592–593*, 728–731. [[CrossRef](#)]